RSC Mechanochemistry

Accepted Manuscript

This article can be cited before page numbers have been issued, to do this please use: S. Das, J. Dolai, B. Mukherjee, A. Maity and N. R. Jana, *RSC Mechanochem.*, 2025, DOI: 10.1039/D5MR00041F.

DOI: 10.1039/D5MR00041F

Ultrasound-based mechanochemical generation of reactive oxygen species from nanoparticle conjugated amyloid fibril

Soumi Das, Jayanta Dolai,* Buddhadev Mukherjee, Anupam Maity,* and Nikhil R. Jana*

School of Materials Science, Indian Association for the Cultivation of Science,

2A & 2B Raja S. C. Mullick Road, Kolkata-700032, India

*Address for correspondence to intjd2@iacs.res.in, rajamaity90@gmail.com and camnrj@iacs.res.in

Abstract. Piezoelectric biomaterials have diverse biomedical applications potential via ultrasound-based wireless mechanochemical reaction at remote area of body/medical device. However, most of the biomaterials have weak piezoelectric property compared to chemically designed piezoelectric materials. In current approach, piezoelectric property of certain biomaterials are enhanced by transforming them into anisotropic fibril/sheet-like morphology. Here, we demonstrate that piezoelectric property of amyloid fibril can be enhanced by 2 times via conjugation with nanoparticle and this can enhance the ultrasound-based mechanochemical production of reactive oxygen species by 4 times. In particular, we have synthesized nanoparticle-conjugated lysozyme fibril with the piezoelectric constant value as high as 82 pm/V. Thin films derived from these materials can generate periodic voltage/current pulse under the exposure of medical grade ultrasound that can reach upto 1 V/15 nA. Colloidal dispersion of these materials generates superoxide/hydroxyl radical via ultrasound-based mechanochemical reaction and degrade dye. This strategy can be adapted to improve the mechanochemical reaction performance of weakly piezoelectric materials.

Keywords. amyloid fibril, piezoelectric, nanoparticle, mechanochemistry, reactive oxygen species

View Article Online
DOI: 10.1039/D5MR00041F

Introduction

Piezoelectric materials produce electric charge in response to applied mechanical stress.[1,2] Inorganic nanocrystal that lacks center of symmetry such as ZnO, $PbZrO_3$, $BaTiO_3$, $ZnSnO_3$ are classic example of piezoelectric nanomaterials.[3,4] These materials have diverse biomedical application potential including drug delivery, tissue engineering, tumor therapy, biosensors and curing of neurodegenerative disease.[5-7] However, cytotoxicity of many of these inorganic nanomaterials restricts their biomedical applications, as their interaction with biological systems can induce harmful side effects.[5] In this context, biomolecule-based piezoelectric materials are envisioned for advanced biomedical applications due to their biocompatibility and flexibility.[8-10] Bone, silk, wood, collagen, tendon, deoxyribonucleic acid (DNA) films are notable examples of naturally occurring piezoelectric biomaterials.[11-15] The piezoelectricity exhibited by these biological components is believed to play a crucial role in maintaining physiological balance in living systems and is closely linked to human health.[10] For example, the piezoelectricity of skin is responsible for converting mechanical stress into electrical signals, which helps in sensory perception. This property also aids in the regulation of various physiological processes by providing feedback on touch and pressure.[13] Additionally, it contributes to the skin's ability to heal and regenerate by influencing cellular activities.[13] Certain amino acids, proteins and polypeptides also exhibit piezoelectricity.[11,12] The anisotropic morphology of fibers and fibrils derived from specific amino acids, peptides, and proteins also exhibits piezoelectric properties.[16] For example, fibrils derived from lysozyme, fluorenyl methyl oxy carbonyl diphenylalanine (Fmoc-FF), cyclic β-peptides showcase piezoelectric property.[17-19] When piezoelectric materials are exposed to ultrasound-based mechanical stress, they generate electric charge and trigger redox reactions with water and dissolved oxygen. This process leads to mechanochemical formation of reactive oxygen species (ROS) such as hydroxyl radical (•OH), superoxide (O_2•$^-$) and hydrogen peroxide

View Article Online
DOI: 10.1039/D5MR00041F

(H_2O_2).[20-22] These generated ROS are used for pollutant degradation, chemical conversion and functional group transformation.[20-22] These processes are commonly called as piezocatalysis. Considering the weak piezoelectric properties of biomaterials various approaches have been adapted for enhancing the piezocatalysis that include increased structural anisotropy or composite formation with nanoparticle/polymer.[18,23,24] These approaches offer more asymmetric arrangement of charges,[18,23] lower the charge recombination processes[23] and induce greater imbalance of charge carriers on the surface of these materials.[23]

We have recently demonstrated that the piezoelectric property of amyloid/protein fibrils can be enhanced by 4-10 times via extension of the β-sheet structure with the piezoelectric constant values in the range of 24-42 pm/V for fibrils and piezoelectric constant value upto 62 pm/V for sheet/bundle-like structures.[18] Considering the fact that amyloid/protein fibrils can be routinely made in vitro with good colloidal property, further enhancement of their piezoelectric property can be beneficial for application point of view. In this context, we have investigated the piezoelectric property of nanoparticle conjugated amyloid fibrils. We demonstrate that piezoelectric property of amyloid fibril can be enhanced by 2 times via conjugation with nanoparticle and the piezoelectric constant value can reach upto 82 pm/V. This enhanced piezoelectric property is shown to enhance the ultrasound-based mechanochemical reactions by 4 times.

View Article Online
DOI: 10.1039/D5MR00041F

Result and Discussion

Nanoparticle attachment enhances the piezoelectric property of amyloid fibril. We have selected lysozyme fibrils as a model amyloid fibril as this fibril and its nanoparticle composites are well studied.[25] (Figure 1a) Lysozyme protein based amyloid fibril has been synthesized using our previously reported method.[18] Silica-coated hydrophilic Fe_3O_4 nanoparticles and histidine coated Au nanoparticles are separately synthesized following reported methods.[23,26] Gold nanoparticles is selected due to the well-known property to enhance photocatalytic processes via lowering of charge carrier recombination[27] and iron oxide is selected due to their well-known Fenton reaction property.[28] Transmission electron microscopy (TEM) of these nanoparticles shows spherical shape with 5-8 nm of core size. (see Supporting Information, Figure S1) Next, nanoparticle composites are prepared by simple mixing of colloidal dispersion of nanoparticles with a colloidal dispersion of amyloid fibril under stirring conditions. (Figure 1a) TEM image shows fibril morphology and attachment of Au/Fe_3O_4 nanoparticles. (Figure 1b-d, and Supporting Information, Figure S2) Such attachment is due to the interaction between zwitterionic surface charge of the fibril and cationic surface charge of metal/metal oxide nanoparticles. X-ray diffraction (XRD) pattern of the composites demonstrate the presence of characteristic reflections for Au/Fe_3O_4 nanoparticles. (Supporting Information, Figure S3)

Next, we have investigated the piezoelectric property of amyloid fibril after the composite formation with nanoparticle via piezoresponse force microscopy (PFM). (Figure 2) The characteristic butterfly loop of amplitude versus bias voltage, along with the phase hysteresis plot, indicates the presence of piezoelectric properties. The slope of amplitude versus bias voltage loop is used to calculate the piezoelectric constant of the samples.[23,24,29] The piezoelectric constants of amyloid fibril, amyloid-Au and amyloid-Fe_3O_4 composites are found to be 41 pm/V, 76 pm/V and 82 pm/V, respectively. It is worth mentioning that attachment of nanoparticle on amyloid fibril results in 2 times enhancement of piezoelectric constant. Such

View Article Online
DOI: 10.1039/D5MR00041F

enhancement is likely due to combination of enhanced imbalance of surface charge along the elongated polar axis and charge reservoir property of metal/metal oxide nanoparticles.[23,24,29]

To gain a deeper understanding of the microstructure-dependent polarization of amyloid fibrils and its composites, the dielectric permittivity has been studied. (Supporting Information, Figure S4) Since the dielectric and piezoelectric properties are closely related therefore an insightful understanding of its frequency dependent dielectric permittivity is examined. The dielectric constant (ε') of the investigated samples were estimated using the following relation:

$$\varepsilon' = (C \cdot t)/(\varepsilon_0 A),$$

where A, t, C, denotes the area, thickness, capacitance of the sample, respectively, and $\varepsilon_0 \sim 8.85 \times 10^{-12}$ F/m (free space permittivity). Results show that amyloid-Fe_3O_4 composite exhibits higher dielectric constant followed by amyloid-Au composite and amyloid fibril.

We have further measured the open circuit voltage and short circuit current of the thin film samples under applied mechanical stress. (Figure 3a, Supporting Information, Figure S5) The current/voltage measurements clearly show the appearance of positive and negative peak that correspond to the immediate response to the applied stress and the material's damping effect, respectively, demonstrating the piezoelectric characteristics of the films. The obtained electrical output for amyloid fibrils and its composites is closely related to piezoelectric constant values, and amyloid-Fe_3O_4 generates the maximum voltage (about 1 V) and maximum current (about 15 nA) followed by amyloid-Au and amyloid fibril. (Figure 3b,c) We have further investigated the application potential of amyloid-Fe_3O_4 composite as human motion sensor. As shown in Figure 3d, the sensor is attached to the finger. When the finger is bent from a relaxed state to a specific angle, piezoelectric signals are achieved and the voltage is amplified with the increasing of angles. These results demonstrate that amyloid fibril-based composites have significant potential for monitoring human motion and enabling various practical self-powered sensing applications in medical devices.

Enhancement of mechanochemical reactive oxygen species (ROS) generation by amyloid fibril after nanoparticle attachment. Next, we have investigated the mechanochemical reaction performance of amyloid fibrils and their nanocomposites using ultrasound. Ultrasound is a unique source in generating periodic mechanical pressure and more importantly, it is used in different medical/therapeutic applications.[5-7] Piezoelectric materials can generate an electric charge when subjected to stress, such as ultrasound. These electrical charges induce redox reactions with water and dissolved oxygen to produce ROS. In this case we have examined the generation of reactive oxygen species (ROS) such as hydroxyl radicals (•OH), superoxide radicals (O_2•$^-$), induced by ultrasound. (Figure 4) Typically, a colloidal dispersion of amyloid fibrils or it's nanocomposite is mixed with terephthalic acid (probe for hydroxyl radical) or nitroblue tetrazolium (NBT) (probe for superoxide radical) and exposed to ultrasound. Next, a part of the reaction mixture is collected at different time points for spectroscopic investigation. (Figure 4a-d) Hydroxyl radicals react with terephthalic acid, leading to the generation of fluorescent 2-hydroxy terephthalic acid (ex: 315 nm, em: 420-430 nm).[21] The increase in emission intensity with ultrasound exposure time is used to quantify the level of hydroxyl radicals generated under the piezocatalytic condition. (Figure 4) Superoxide radicals react with NBT, leading to a decrease in the UV-visible absorption peak of NBT at 259 nm due to the production of an insoluble bright blue formazan product.[21] The decrease in absorbance with increasing ultrasound exposure time is utilized to quantify the level of superoxide radicals under the piezocatalytic condition. (Figure 4) We have three distinct observations. First, ROS generation capability of amyloid fibril increases significantly after the attachment of gold/Fe_3O_4 nanoparticles and Fe_3O_4 nanoparticle offer better enhancement of mechanochemical ROS generation. (Figure 4a-d) Both assays indicate that the amyloid-Fe_3O_4 composite generates the highest amount of hydroxyl and superoxide radicals, followed by the amyloid-Au composite and amyloid fibrils, under similar experimental conditions. Control

View Article Online
DOI: 10.1039/D5MR00041F

experiments indicate that either ultrasound alone or Au/Fe_3O_4 nanoparticles generates only a minimal amount of ROS under similar experimental conditions. (Supporting Information, Figure S6)

Second, there is a correlation between piezoelectric constant and mechanochemically generated ROS. It is expected that a higher piezoelectric constant enhances charge migration, thereby improving mechanochemical ROS generation performance.[24] Hence, the amyloid-Fe_3O_4 composite with highest piezoelectric constant demonstrates highest ROS generation capability. The presence of metal/metal oxide nanoparticle on amyloid fibril promotes the efficient separation of charge carriers under piezocatalytic condition and increases the availability of electrons and holes to participate in redox reactions.[23] Hence, attachment of metal/metal oxide nanoparticle on amyloid fibril enhances the piezocatalytic ROS generation. Thirdly, mechanochemically generated ROS-assisted degradation performance of rhodamine B is enhanced by 4 times after nanoparticle conjugation. (Figure 5a-d) It was found that amyloid-Fe_3O_4 composite shows highest rhodamine B degradation efficiency (80 %) followed by amyloid-Au composite and amyloid fibril under the similar experimental condition. The kinetics of dye degradation can be described by a linear relationship between $\ln(C_0/C)$ and ultrasound exposure time, from which the rate constant of the degradation process have been determined. (Figure 5d) The rate constant values for the degradation of rhodamine B is 0.004 min^{-1}, 0.01 min^{-1} and 0.016 min^{-1} for amyloid fibril, amyloid-Au and amyloid-Fe_3O_4, respectively. (Figure 5d) This result suggests that rhodamine B degradation is 4 time faster after Fe_3O_4 conjugation on amyloid fibril. The observed mechanochemical dye degradation performance is comparable with the reported piezocatalytic and photocatalytic performances.[30-37] (see Supporting Information, Table S1)

Electron spin resonance (ESR) spectra are further recorded to confirm the formation of ROS by amyloid-Fe_3O_4 under the ultrasound exposure. (Figure 6a,b) 5,5-Dimethyl-1-pyrroline *N*-

View Article Online
DOI: 10.1039/D5MR00041F

oxide (DMPO) is used as a spin-trapping agent for detecting the hydroxyl (•OH) and superoxide (O_2•$^-$) radicals. We have observed the four characteristic signature peaks (1:1:1:1) of the DMPO-O_2•$^-$ adduct in a DMSO solvent and four characteristic signature peaks (1:2:2:1) of the DMPO-•OH adduct in a water solvent. These ESR results demonstrate the formation of superoxide and hydroxyl radicals under the mechanochemical reaction condition. Control experiments show that the absence of ultrasound or the absence of amyloid-Fe_3O_4 cannot produce these ROS. We have also studied the stability of the nanocomposites after exposure of ultrasound. Fibril-bound nanoparticles are quantified using inductively coupled optical emission spectrometry (ICP-OES) showing that nanocomposites retain the content of Au/Fe even after 2h of ultrasound exposure. (Supporting Information, Figure S7) TEM images also suggest that the nanocomposites retain their morphology after 2h of ultrasound exposure. (Supporting Information, Figure S8) These results suggest that the binding of Au/Fe_3O_4 nanoparticles to amyloid fibrils is stable enough against the mechanical stress.

Conclusion

We have demonstrated that nanoparticle conjugation can enhance the piezoelectric property and mechanochemical reaction performance of amyloid/protein fibrils by 2-4 times. In particular, we have shown that piezoelectric property of nanoparticle-conjugated lysozyme fibril can be as high as 82 pm/V. Thin films derived from these materials can generate periodic voltage/current pulse under the exposure of medical grade ultrasound that can reach upto 1 V/15 nA. Ultrasound exposure of colloidal dispersion of these materials generate reactive oxygen species via mechanochemical reaction and degrade dye. Although reactive oxygen species can be generated by iron oxide in presence of hydrogen peroxide,[38,39] present approach offers advantage as reactive oxygen species can be generated in presence of oxygen and water and in absence of any hydrogen peroxide. This strategy can be adapted to improve the mechanochemical reaction performance of weakly piezoelectric materials.

View Article Online
DOI: 10.1039/D5MR00041F

The observed piezoelectricity of amyloid fibrils has intriguing physiological implications considering the reported mechanical and electrical influence on these protein structures.[40-42] In particular, the piezoelectric properties of amyloid fibrils open up possibilities for therapeutic interventions. For example, external mechanical or electrical stimuli could be used to modulate their behavior or breaking them down, potentially preventing their accumulation in tissues.[41,42] Given the broad range of biomedical applications for piezoelectric materials, such as wireless activation of neuronal cells,[43] cell differentiation,[44] electroporation[45] and tumor/cell therapy,[46] these piezoelectric fibril composites could be developed for similar uses.

ASSOCIATED CONTENT

Supporting Information

Synthesis details of amyloid fibril and nanoparticle composite with amyloid fibrils, experimental procedure for ultrasound-based mechanochemical reaction and additional materials characterization data. This material is available free of charge via the Internet at http://pubs.acs.org.

Notes

The authors declare no competing financial interests.

Acknowledgement

NRJ acknowledges DST-SERB (SPR/2021/000011), Government of India for financial assistance. JD acknowledges CSIR and BM acknowledges UGC, government of India for providing research fellowship.

References

1. Z. L. Wang, J. Song, *Science* 2006, **312 (5771)**, 242-246.

View Article Online
DOI: 10.1039/D5MR00041F

2. X. Wang, J. Song, J. Liu, Z. L. Wang, *Science* 2007, **316**, 102-105.

3. 1. S. Li, Z. Zhao, J. Zhao, Z. Zhang, X. Li, J. Zhang, *ACS Appl. Nano Mater.* 2020, **3**, 1063-1079.

4. S. D. Mahapatra, P. C. Mohapatra, A. I. Aria, G. Christie, Y. K. Mishra, S. Hofmann, V. K. Thakur, *Adv. Sci.* 2021, **8**, 2100864.

5. A. Cafarelli, A. Marino, L. Vannozzi, J. Puigmartí-Luis, S. Pané, G. Ciofani, L. Ricotti, *ACS Nano* 2021, **15**, 11066-11086.

6. J. Dolai, A. Biswas, N. R. Jana, *ACS Appl. Nano Mater.* 2022, **5**, 14038-14050.

7. J. Ouyang, Z. Tang, N. Farokhzad, N. Kong, N. Y. Kim, C. Feng, S. Blake, Y. Xiao, C. Liu, T. Xie, W. Tao, *Nano Today* 2020, **35**, 100949.

8. D. Kim, S. A. Han, J. H. Kim, J.-H. Lee, S.-W. Kim, S.-W. Lee, *Adv. Mater.* 2020, **32**, 1906989.

9. R. Wang, J. Sui, X. Wang, *ACS Nano* 2022, **16**, 17708-17728.

10. S. Chen, X. Tong, Y. Huo, S. Liu, Y. Yin, M.-L. Tan, K. Cai, W. Ji, *Adv. Mater.* 2024, 2406192.

11. E. Fukada, *Wood Sci. Technol.* 1968, **2 (4)**, 299-307.

12. C. A. L. Bassett, R. O. Becker, *Science* 1962, **137**, 1063-1064.

13. H. Athenstaedt, H. Claussen, D. Schaper, *Science* 1982, **216**, 1018-1020.

14. W. S. Williams, L. Breger, *J. Biomech.* 1975, **8 (6)**, 407-413.

15. E. Fukada, Y. Ando, *J. Polym. Sci. Part A-2: Polym. Phys.* 1972, **10**, 565-567.

16. M. Minary-Jolandan, M.-F. Yu, *ACS Nano* 2009, **3**, 1859-1863.

17. K. Ryan, J. Beirne, G. Redmond, J. I. Kilpatrick, J. Guyonnet, N.-V. Buchete, A.L. Kholkin, B. J. Rodriguez, *ACS Appl. Mater. Interfaces* 2015, **7**, 12702-12707.

18. J. Dolai, A. Maity, B. Mukherjee, R. Ray, N. R. Jana, *ACS Appl. Mater. Interfaces* 2024, **16 (1)**, 217-227.

19. T. Kurita, T. Terabayashi, S. Kimura, K. Numata, H. Uji, *Biomacromolecules* 2021, **22 (7)**, 2815-2821.

20. W. Qi, Y. Fu, E. Liu, Z. Cheng, Y. Sun, S. Liu, M. Yang, *EES Catalysis* 2024, **2 (4)**, 884-910.

21. J. Dolai, A. R. Sarkar, S. Das, N. R. Jana, *Part. Part. Syst. Charact.* 2023, **40 (12)**, 2300065.

22. S. Asgari, G. Mohammadi Ziarani, A. Badiei, S. Iravani, *Mater. Adv.* 2023, **4 (23)**, 6092-6117.

23. J. Dolai, A. Biswas, R. Ray, N. R. Jana, *ACS Appl. Mater. Interfaces* 2022, **14**, 26443-26454.

24. X. Zhou, B. Shen, A. Lyubartsev, J. Zhai, N. Hedin, *Nano Energy* 2022, **96**, 107141.

25. K. Debnath, A. K. Sarkar, N. R. Jana, N. R. Jana, *Acc. Mater. Res.* 2022, **3**, 54−66.

26. N. R. Jana, P. K. Patra, A. Saha, S. K. Basiruddin, N. Pradhan, *J. Phys. Chem. C 2009*, **113**, 21484–21492.

27. V. Subramanian, E. E. Wolf, P. V. Kamat, *J. Am. Chem. Soc.* 2004,**126**, 4943-4950.

28. S. Pal, N.R. Jana, *ACS Appl. Nano Mater.* 2020, **3,** 2, 1683-1692.

29. L. Cai, J. Du, F. Han, T. Shi, H. Zhang, Y. Lu, S. Long, W. Sun, J. Fan, X. Peng, *ACS Nano* 2023, **17 (8)**, 7901-7910.

30. C. Porwal, M. Sharma, R. Vaish, V. S. Chauhan, *ACS Appl. Eng. Mater.* 2023, **1 (1)**, 295-303.

31. A. Shukla, A. Gaur, S. Dubey, R. Vaish, *RSC Mechanochem.* 2024, **1**, 465-476.

32. A. Biswas, S. Saha, S. Pal, N. R. Jana, *ACS Appl. Mater. Interfaces* 2020, **12 (43)**, 48363-48370.

33. M. Ismail, Z. Wu, L. Zhang, J. Ma, Y. Jia, Y. Hu, Y. Wang, *Chemosphere* 2019, **228**, 212-218.

34. A. Mehrehjedy, P. Kumar, Z. Ahmad, P. Jankoski, A. S. Kshirsagar, J. D. Azoulay, X. He, M. K. Gangishetty, T. D. Clemons, X. Gu, W. Miao, S. Guo, *ACS Omega,* 2024, **9**, 49239−49248.

35. H. Lu, L. Zhang, J. Ma, N. Alam, X. Zhou, Y. Ni, *Nanomaterials,* 2019, **9(2)**, 277.

36. Y. Zhou, J. Shen, Y. Bai, T. Li, G. Xue, *Int. J. Biol. Macromol.*, 2020, **152**, 242–249.

37. E. Ravelo-Nieto, S. A. Ovalle-Serrano, E. A. Guti´errez-Pineda, C. Blanco-Tirado, M. Y. Combariza, *J. Environ. Chem. Eng.,* 2023, **11**, 109516.

38. K. Zhang, Z. Yang, X. Meng, Y. Cao, Y. Zhang, W. Dai, H. Lu, Z. Yu, H. Dong, X. Zhang, *Mater. Chem. Front*., 2018, **2**, 1184-1194.

39. N. Jaafarzadeh, A. Takdastan, S. Jorfi, F. Ghanbari, M. Ahmadi, G. Barzegar, *J. Mol. Liq.,* 2018, **256**, 462-470.

40. A. Kozell, D. Eliaz, A. Solomonov, D. Benyamin, G. Shmul, O. Brookstein, I. Rosenhek-Goldian, U. Raviv, U. Shimanovich, *Proc. Nat. Acad. Sci.* **2023,** *120*, e2212849120.

41. S. Kalita, H. Bergman, K. D. Dubey, S. Shaik, *J. Am. Chem. Soc.* **2023,** *145* (6), 3543-3553.

42. I. Rosales, L. Salazar, D. Luna, A. Negrón, I. Bdikin, B. Rodriguez, and A. Heredia, *Am. J. Mol. Biol*., **2021**, *11*, 1-14.

43. A. Marino, S. Arai, Y. Hou, E. Sinibaldi, M. Pellegrino, Y.-T. Chang, B. Mazzolai, V. Mattoli, M. Suzuki, G. Ciofani, *ACS Nano* **2015,** *9*, 7678-7689.

44. G. G. Genchi, L. Ceseracciu, A. Marino, M. Labardi, S. Marras, F. Pignatelli, L. Bruschini, V. Mattoli, G. Ciofani, *Adv. Healthcare Mater.* **2016,** *5*, 1808-1820.

45. J. Dolai, A. R. Sarkar, A. Maity, B. Mukherjee, N. R. Jana, *ACS Appl. Mater. Interfaces* **2023,** *15* (51), 59155-59164.

46. P. Zhu, Y. Chen, J. Shi, *Adv. Mater.* **2020,** *32*, 2001976.

View Article Online
DOI: 10.1039/D5MR00041F

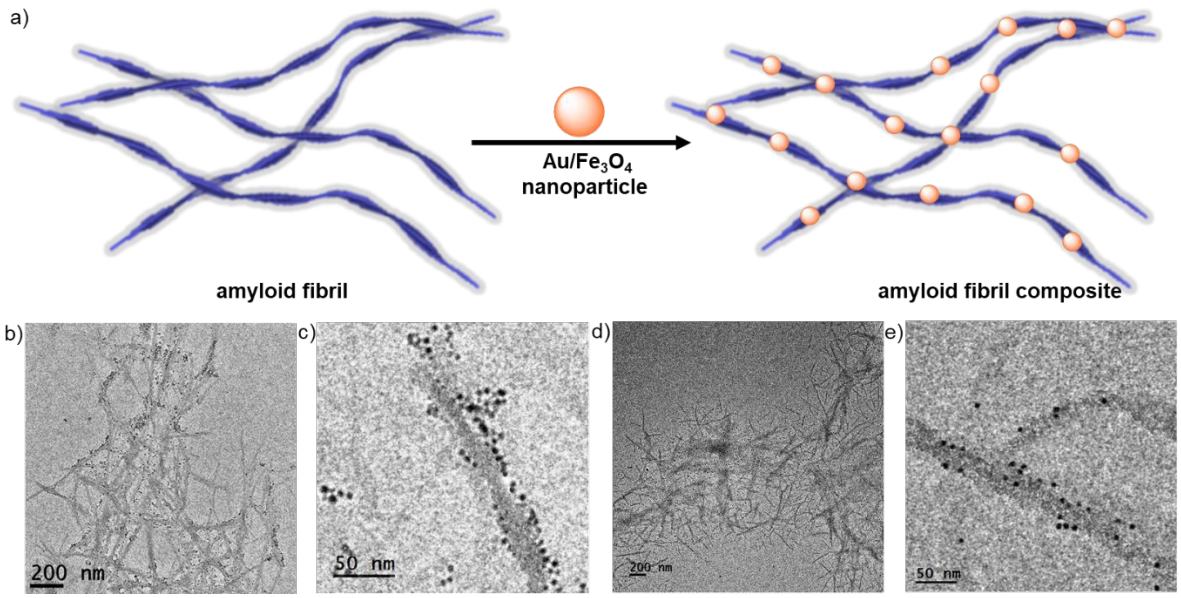

Figure 1. (a) Schematic presentation of amyloid fibril and its gold/iron oxide composites. (b-d) Transmission electron microscopy (TEM) image of amyloid-Au (b,c) and amyloid-Fe_3O_4 (d,e) composites. The magnified images demonstrate the attachment of Au/Fe_3O_4 nanoparticles with amyloid fibril.

View Article Online
DOI: 10.1039/D5MR00041F

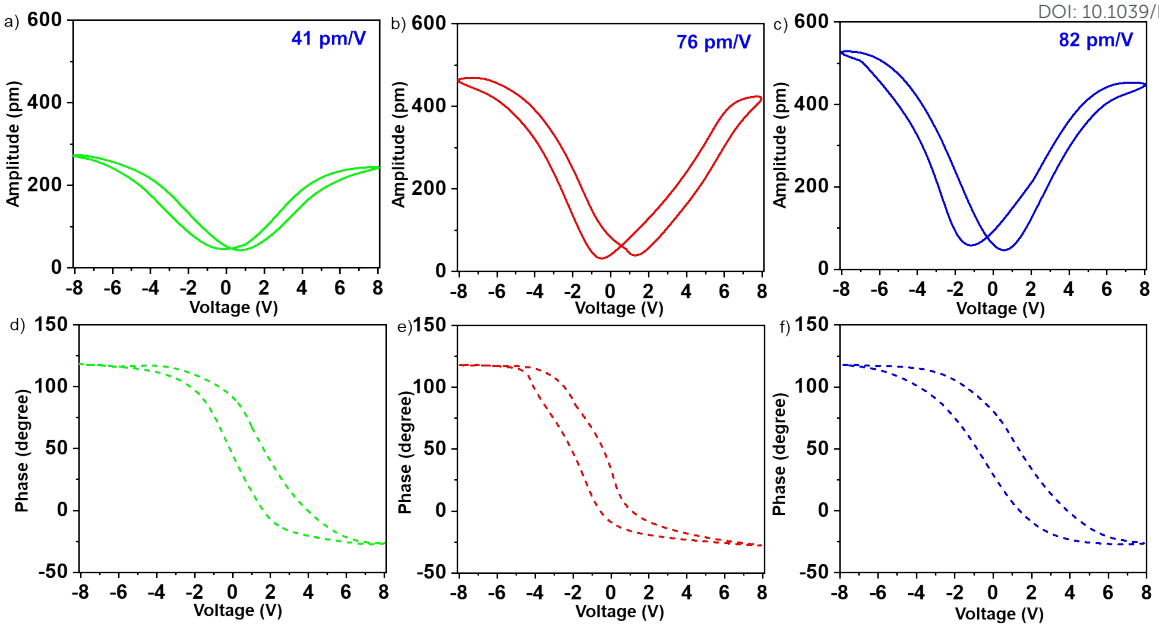

Figure 2. (a-c) Amplitude-voltage butterfly loop of amyloid fibril (a), amyloid-Au (b) and amyloid-Fe_3O_4 (c) with piezoelectric constant values in the inset. (d-e) Phase hysteresis loop of amyloid fibril (a), amyloid-Au (b) and amyloid-Fe_3O_4 (c).

View Article Online
DOI: 10.1039/D5MR00041F

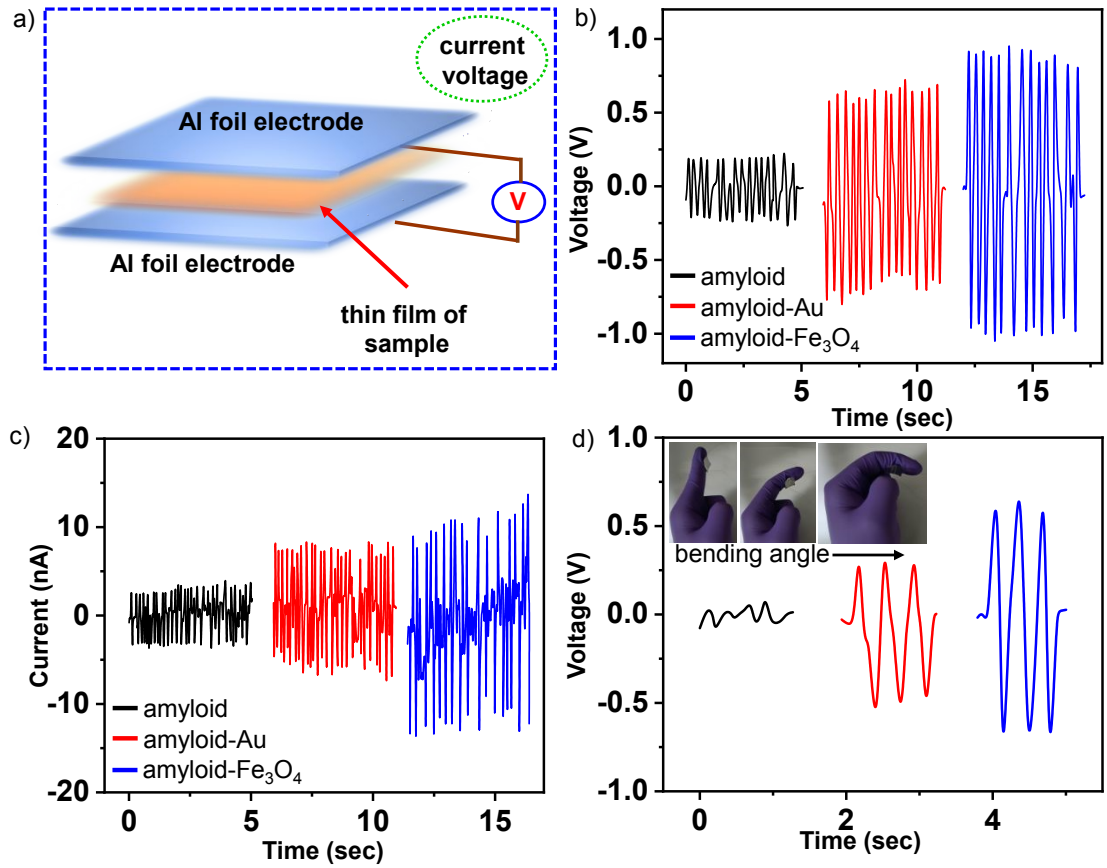

Figure 3. a) Schematic representation of the experimental setup for piezo-current and piezo-voltage measurement. b,c) Piezoelectric response of amyloid fibrils and its composites measured using mechanical stress: (b) piezo-voltage and (c) piezo-current. d) Piezo-voltage response patterns of the amyloid-Fe_3O_4 composite sensor fixed on a finger under different bending degrees.

View Article Online
DOI: 10.1039/D5MR00041F

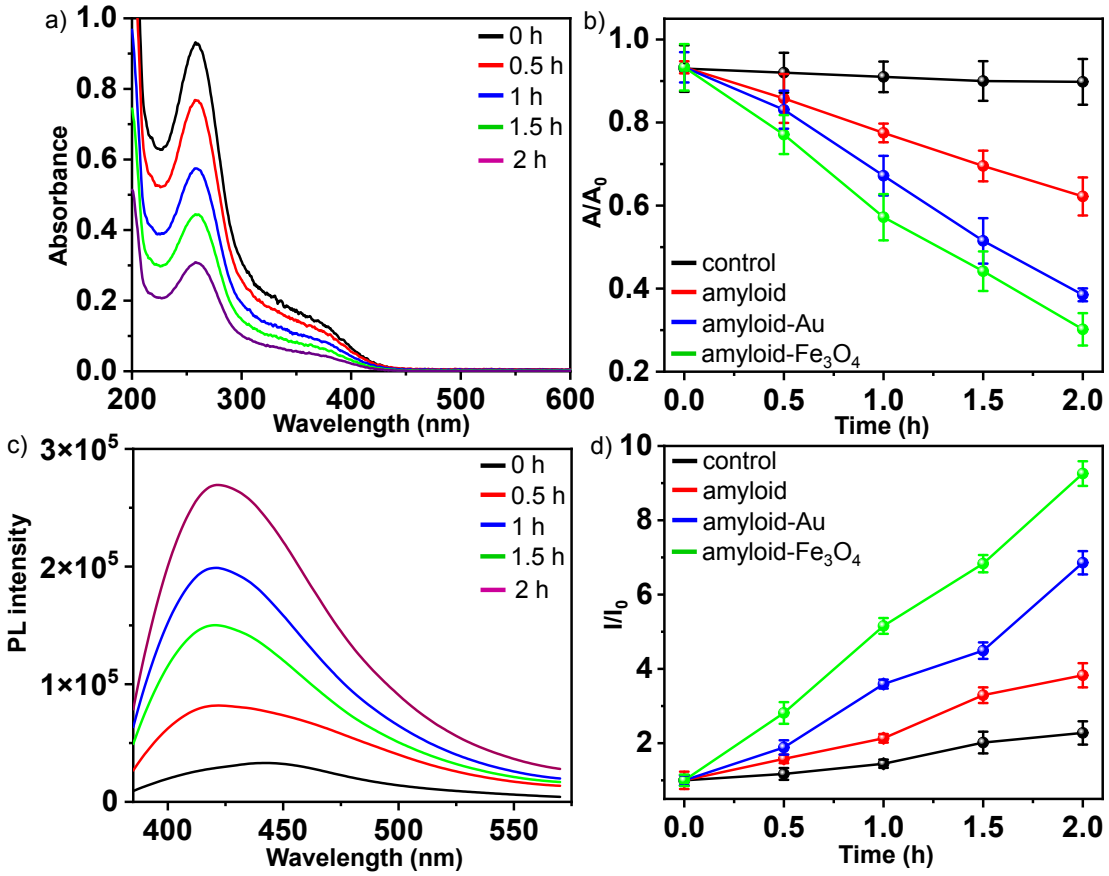

Figure 4. Evidence of ROS generation by colloidal amyloid fibril and its composites (1 mg/mL) under ultrasound exposure. (a) NBT absorbance-based detection of superoxide radicals produced by the amyloid-Fe_3O_4 composite, which decreases with ultrasound exposure time. (b) Enhanced superoxide radical generation by amyloid fibril after composite formation with nanoparticle. Here, A/A_0 is the ratio of the absorbance of NBT after and before ultrasound exposure. (c) Terephthalic acid emission-based detection of hydroxyl radicals produced by the amyloid-Fe_3O_4 composite, which increases with ultrasound exposure time. (d) Enhanced hydroxyl radical generation by amyloid fibril after composite formation with nanoparticle. Here, I/I_0 is the ratio of the fluorescence intensity of terephthalic acid after and before ultrasound exposure. An ultrasonic transducer with 120 W power and 33 kHz frequency is used for all of these measurements. Error bar represents the mean of three independent experiments.

View Article Online
DOI: 10.1039/D5MR00041F

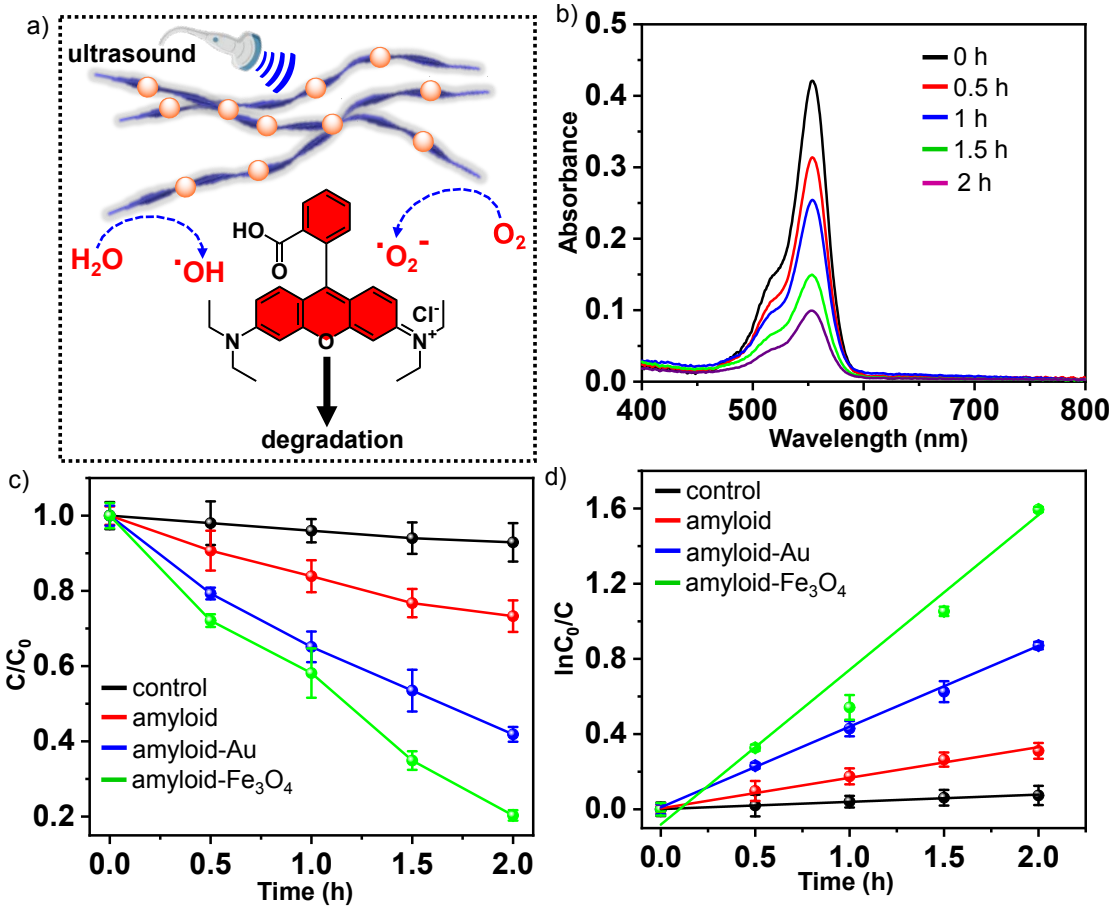

Figure 5. (a) Schematic representation of rhodamine B degradation using amyloid fibril-based colloidal nanocomposite. (b) Rhodamine B degradation by amyloid-Fe_3O_4 composite in the presence of ultrasound exposure as observed by a progressive decrease of rhodamine B absorbance. (c) Rhodamine B degradation kinetics in the presence of amyloid fibril and its composite with nanoparticle. Control represents the degradation of rhodamine B with ultrasound. (d) Plot of $\ln(C_0/C)$ vs time using different piezocatalyst. An ultrasonic transducer with 120 W power and 33 kHz frequency is used for all of these measurements. Error bar represents the mean of three independent experiments.

View Article Online
DOI: 10.1039/D5MR00041F

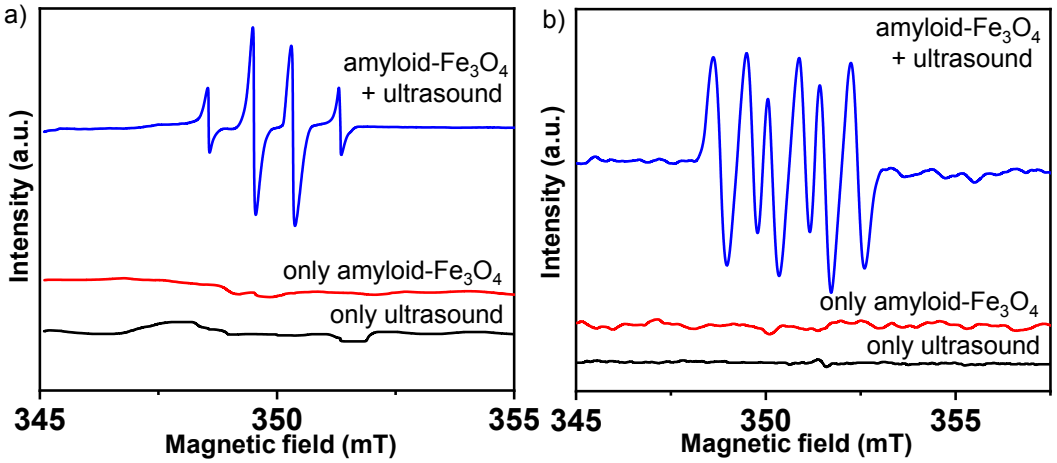

Figure 6. ESR spectra of DMPO-trapped ROS species generated by amyloid-Fe_3O_4 composite under ultrasonic vibration. Four characteristic signature peaks (1:1:1:1) of DMPO-O_2•$^-$ adduct in a DMSO solvent (i) and four characteristic signature peaks (1:2:2:1) of DMPO-•OH adduct in water solvent (ii) suggest the formation of superoxide/hydroxyl radicals. Control experiments show that absence of ultrasound or absence of amyloid-Fe_3O_4 cannot produce these ROS.

View Article Online
DOI: 10.1039/D5MR00041F

The data supporting this article have been included as part of the Supplementary Information.